Active nonperturbative stabilization of the laser-plasma-accelerated electron beam source

Curtis Berger,* Sam Barber, Fumika Isono, Kyle Jensen, Joseph Natal, Anthony Gonsalves, and Jeroen van Tilborg

Lawrence Berkeley National Laboratory, Berkeley, California 94720, USA

(Received 27 October 2022; accepted 22 February 2023; published 15 March 2023)

Laser plasma accelerators have the ability to produce high-quality electron beams in compact, all-optical-driven configurations, with the electron beams uniquely suited for a wide variety of accelerator-based applications. However, fluctuations and drifts in the laser delivery to the mm-scale plasma target (the electron beam source) will translate into electron beam source variations that can limit their utility for demanding applications like light sources. Based on previous work in developing a nonperturbative diagnostic for the high-power laser delivery at focus [1], we present a full four-dimensional active-stabilization system for the laser (transverse laser focus position and laser pointing angle in both transverse planes) and experimentally demonstrate how, as a result of the laser stabilization, critical parameters in the electron beam source were stabilized. Through the use of an energy resolved imaging system for the electron beam, we directly monitor the jitter in the transverse electron beam source location. Furthermore, the dispersion in the orthogonal plane to the magnetic spectrometer was recorded for each shot which is tied to the source pointing angle of the electron beam and, in part, driven by the angle of the laser at the interaction point. Our laser stabilization system reduced variation in the electron beam source location from ~ 12 to 3 μm and reduced the dispersion jitter of the electron beam by 20%.

DOI: 10.1103/PhysRevAccelBeams.26.032801

I. INTRODUCTION

Laser plasma accelerators (LPAs) provide a means for achieving electron beams (e-beams) of multi-MeV to GeV energy levels through the mm-scale acceleration of charged particles via laser-driven plasma wakefields [2–7]. The e-beam quality can match that realized with conventional radio frequency (rf) based particle accelerators, with added advantages of compactness, cost, and intrinsic femtosecond synchronization to other hyperspectral sources. The ultrashort high-peak-current nature of LPA beams can enable novel light sources, attracting interest in developing betatron x rays [8] for applications like bioimaging [9], x-ray free-electron lasers for nonlinear dynamics and single-shot imaging [10], and Compton/Thomson-scattered gamma-ray and x-ray sources for medical and nuclear security applications [11,12]. Plasma based colliders are also a candidate for a future high energy collider [13].

Despite LPAs offering promising applications, using them as alternatives to conventional rf linacs presents several unique challenges that must be addressed. For example, in contrast to a standard rf photoinjector, beams generated in plasma wakefields are typically micron scale in all spatial dimensions. The initial trajectory of these beams is strongly tied to the propagation and evolution of the wakefield, which itself is predominantly determined by the angle and position of the wakefield driving laser. Naturally then, the transverse stability of the LPA-generated beams is strongly coupled to the stability of the drive laser.

Future applications of LPAs like colliders and XFELs require transverse jitter of the electron beam to be a small fraction of the electron beam size. This fact, coupled with the micron scale source size, implies micron to submicron transverse jitter of the drive laser at focus will be required. Given that a focused laser driver is tens of microns in transverse size, drive lasers will need to be stabilized to a fraction of a percent of a beam size [14,15].

Sources of perturbations that lead to LPA drive laser instability include environmental vibrations that couple into optical components, thermal variations to optical surfaces, and open-air turbulence. In addition, thermal drifts inside laser progenitor cavities result in long-term drift of the propagating laser field. The resolved frequency content of these fluctuations has been shown to exceed 100 Hz in the position spectrum and approach 10 Hz in the angle

*Corresponding author.
curtisberger@lbl.gov

spectrum [1]. Thus, the need to integrate high bandwidth stabilization systems into LPAs to correct these fluctuations has become increasingly necessary.

To date, the ability to actively stabilize 100-TW-class laser systems has been investigated in limited quantity. Most notable for 100-TW-class systems is the pioneering work in Ref. [16]. Unlike our work, Ref. [16] required the use of several reflective mirrors and lenses after the interaction point and its impact on the LPA electron beam production was not investigated. Furthermore, the stabilization-driving laser was not intrinsically copropagating with the amplified pulses but was rather derived through postamplifier insertion of a laser pickoff beamline (thus increasing the noncommon path). Additional work on LPA and e-beam stability/control has been investigated [17–22]. Although high-bandwidth active correction has not yet been pursued in these studies, they do highlight the need for the continual development of related active stabilization technologies. In the same spirit then, in this paper, we demonstrate substantial improvement in the transverse stability of LPA-generated e-beams achieved through integration of a nondestructive fast active-feedback system to stabilize a high-power wakefield driver. Stabilizing the focus location results in nearly a factor of 4 improvement of the positional jitter of the e-beam source location with 3-μm rms variation measured over the course of 1 h. Fluctuations in e-beam dispersion were reduced by 20%, whereas the laser angle fluctuations were reduced by an order of magnitude. For both positional and angular jitter, slow drifts (< 1 Hz) as well as shot-to-shot jitter at frequencies up to 20 Hz are nearly eliminated. This is an important step in improving e-beam source stability in LPAs which will result in improved accelerator performance and help bridge the gap from proof-of-concept designs to real-life applications [23–25].

II. EXPERIMENTAL CONFIGURATION

Shown in Fig. 1 is a diagram of a 100-TW class pulsed laser system in use at the BELLA Center for the production and study of electron beams produced by LPAs. The system uses a multistage titanium sapphire chirped pulse for amplification. It starts with an 80-MHz oscillator which is amplified at 1 kHz to 2 mJ in a regenerative amplifier. Further amplification at 1 Hz to 4J is achieved through the use of three multipass amplifiers after the pulse has been stretched to 300 ps. The beam is then compressed back to 40 fs FWHM and focused using an $f/30$ off-axis parabola (OAP), resulting in an on-target energy of ≈ 2.5 J, a focal spot size of 40 μm (FWHM), and a normalized laser strength parameter of $a0 \simeq 1.3$.

Integrated into the OAP chamber shown in Fig. 1 is a wedged fused silica mirror (yellow optic in the figure) with reflective coatings of 99.0% and $> 99.5\%$ (nominal high reflector) for the front and back surface, respectively. This optic was designed such that the front surface and back surface reflections are exactly overlapped on the surface of the OAP with 1.21° angular separation. The back surface reflection, referred to herein as the ghost beam, has a relative attenuation factor compared to the front surface reflection of $\approx 10^{-4}$. The angular separation of the ghost beam allows us to pick it off near the focus and nondestructively monitor the transverse-spatial information of the main kHz pulse train [1] thereby allowing the integration of an active feedback stabilization system and other monitoring diagnostics.

Because of the difference in angle of incidence onto the OAP, the ghost beam does acquire a slight astigmatism, which has negligible impact on the overall stabilization system. We also note that this issue of astigmatism could be avoided by moving the wedged optic to the location of the final steering mirror. However, at this location, the laser fluence is highest and the special coatings required to create a ghost beam of sufficient energy run the risk of becoming damaged.

The ghost beam diagnostics setup shown in the inset of Fig. 1 contains a 50/50 beam splitter that creates two copies of the ghost beams used for two principle measurements: (i) The reflected ghost beam is directed onto two CCD cameras triggered at 1 Hz for monitoring the near and far field ghost beam copy of the main amplified pulse (Fig. 2) while (ii) the transmitted ghost beam is directed into position sensitive detectors (PSD) used for the feedback stabilization system. A fast mechanical shutter was installed to shield the PSDs from the amplified pulse. The PSDs have 9×9 mm chips with ≈ 0.5 μm resolution and are used to monitor the transverse position and angle of the laser at focus. These two PSDs are part of a commercially available stabilization system (ALIGNA-4D) provided by TEM Messtechnik which includes a 10-kHz PID-feedback-loop microcontroller and the two corrective optics highlighted green in Fig. 1. The stabilization system stabilizes the main 1-Hz high power pulse laser by taking advantage of the quasiperfect correlation in position and angle between the nonamplified mJ background pulse train and the high power wakefield driving 1-Hz pulse laser [1]. The corrective optics are equipped with both stepper motors for course adjustment and stacked piezos for fine adjustment. The location of these optics was strategically chosen to minimize coupling between position and angle when applying corrections. If the first (upstream) corrective optic is given a 1-μrad tilt, it moves the transverse focus location by ≈ 0.85 μm and introduces a ≈ 6-μrad tilt at focus. Likewise, a 1-μrad tilt applied to the second (downstream) corrective optic, results in focal position and angle changes ≈ 2 μm and 1 μrad, respectively. In other words, the first corrective optic primarily corrects the angle at focus while the second optic corrects primarily position at focus. It is worth noting that the choice of position for the two corrective optics was also motivated by the minimum size of the optics at the two locations −3” and 4”,

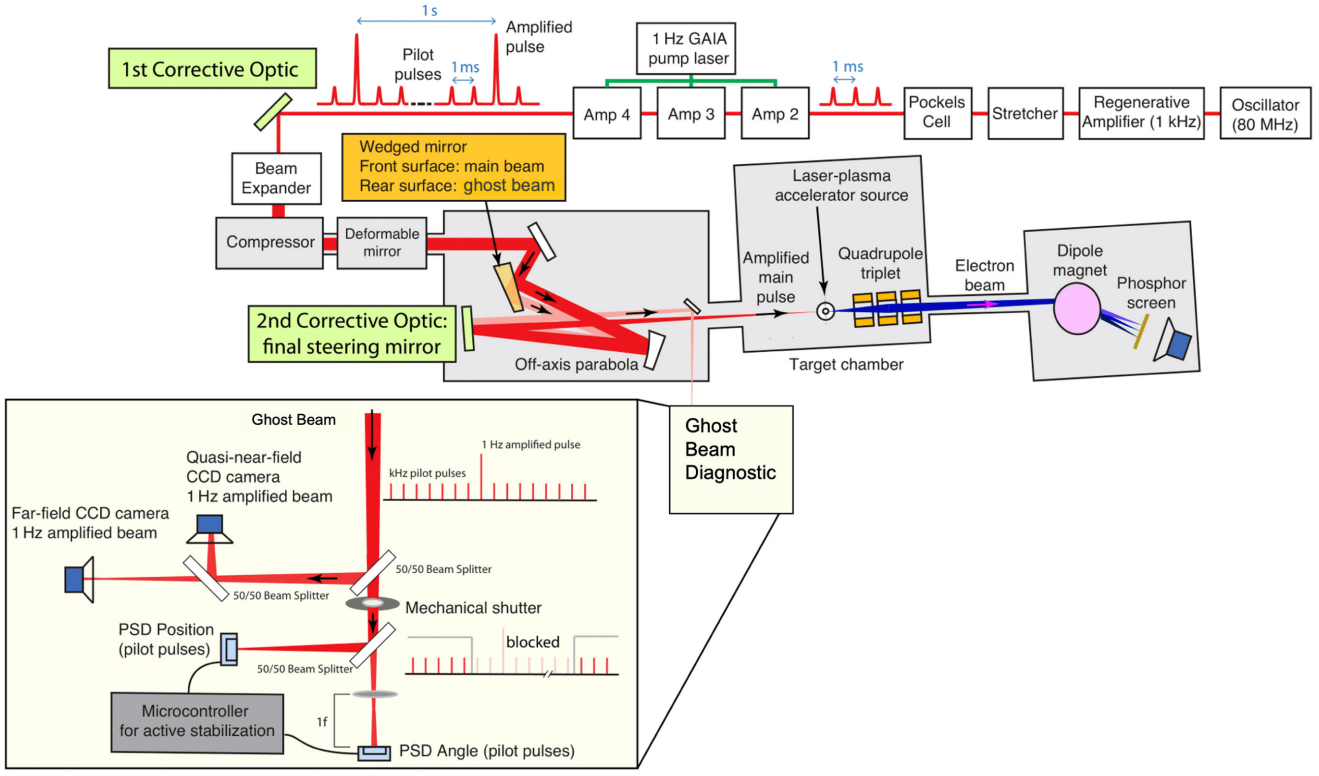

FIG. 1. Top-down schematic overview of the hundred terawatt undulator (HTU) experimental setup. The front end of the laser indicated by the first four boxes in the top right delivers a 1-kHz pulse train, of which 1 in every 1000 pulses is amplified by the Amp2-Amp3-Amp4 amplifiers. The copropagating amplified and nonamplified (pilot) pulses are routed through an optical system that includes mirrors, lenses, corrective mirrors, a wedged mirror, and a parabola, among others. The wedged mirror delivers a correlated copy (referred to as a ghost beam) of the laser's final focus to the ghost beam diagnostics. The latter setup diagnoses the position and pointing fluctuations of the laser, with the corrective optics driving the active stabilization for both position and angle in both transverse coordinates x and y. The 100-MeV class electron beam produced at the laser-plasma interaction point is imaged with a quadrupole triplet system onto the dispersive plane of a magnetic spectrometer, thus yielding the electron source position and dispersion in the vertical y plane (out of plane of the setup drawing).

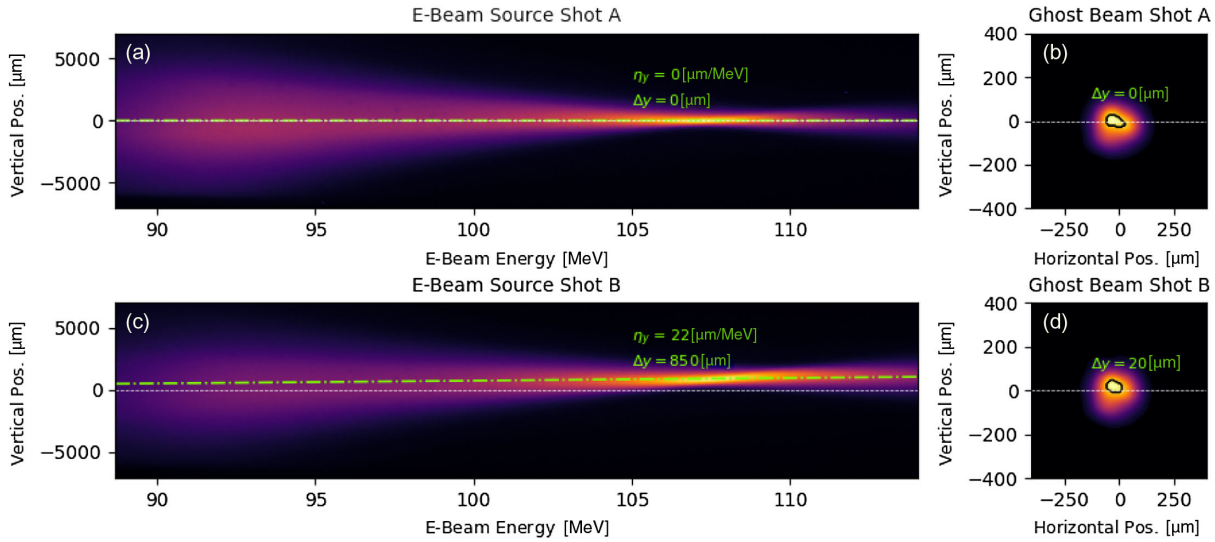

FIG. 2. Shot-to-shot fluctuations of the 1-Hz ghost beam copy (b and d) and the e-beam source (a and c) imaged into the magnetic spectrometer is shown when active stabilization is turned off. The dashed white-colored horizontal lines indicate a nominal design axis while the dashed green-colored lines in plots a and c display the angular tilt of the e-beam brought about by energy-dependent dispersion. We note the intrinsic instabilities present during shot-to-shot firing of an experimental run.

respectively. With a PID feedback rate of 10 kHz, the stabilization system will be largely limited by the bandwidth limitations of the two corrective mounts which will be dependent upon their mass. The associated bandwidths for the 3" and 4" mirror mount were measured to be around 60 and 20 Hz, respectively. We note that engineering improvements to the 4" mount are forthcoming and are expected to extend the mechanical bandwidth to match the 3" optic mount.

III. ELECTRON BEAM GENERATION AND TRANSPORT

Electron beams are generated in the target chamber where the main beam is focused onto a supersonic gas jet target with an ~ 800-μm opening diameter and a throat size of 500 μm. The gas used for the target was fed at 400 psi and is a 99% He and 1% N_2 mixture, which is widely used to produce electron beams via ionization injection [26,27]. We are able to measure pertinent aspects of the electron beam source through the use of our dedicated transport line, which consists of a permanent magnet quadrupole (PMQ) triplet that focuses the electron beam into a magnetic spectrometer. We discuss here certain salient aspects of this transport which allow the measurement of the electron beam source location and exit angle.

Using the standard approach to charged particle beam optics, the transport line for the electron beams can be represented by a generalized transfer matrix, R, which is a function of e-beam energy and the various magnetic elements in the line. This matrix is specified to transform the vector representing a particle's position, angle, and energy from one point along a beamline to another. In the case at hand, the transport line is rather simple consisting of a single PMQ triplet, drift spaces, and a magnetic dipole used for the spectrometer. Using this approach, we can relate a particle's final position in the magnetic spectrometer to its initial vector. For example, given a particle with energy γ and with initial vertical position y_i and vertical angle y_i' at the LPA source location, we can write its final vertical location y_f in the magnetic spectrometer:

$$y_f(\gamma) = [R_{33}(\gamma)]y_i + [R_{34}(\gamma)]y_i', \tag{1}$$

The special case of $R_{34} = 0$ indicates that point-to-point imaging is satisfied in the vertical plane. In other words, at a specific energy, a particle's final vertical position is only a function of its initial vertical position. The design of our full transport line results in $R_{34}(\gamma)$ which is roughly linear between 80 and 120 MeV with $R_{34} = 0$ for an energy of approximately 108 MeV. Therefore, the measurement of the vertical position of the electron beam at the imaged energy (108 MeV) is a direct measure of the source location magnified by the corresponding R_{33} value. We can express this in equation form as follows:

$$y_f(\gamma_0) = R_{33}(\gamma_0) \times y_i(\gamma_0), \quad \text{with} \quad y_i(\gamma_0) = y_{\text{laser}} + f(\mathcal{O}), \tag{2}$$

Although it is a good assumption that the electron beam source location is one-to-one correlated with the drive laser focal location, secondary effects incorporated in $f(\mathcal{O})$, such as off-axis injection, may cause a slight variation.

To an extent, the exit angle of the electron beam will also be encoded in the beam profile in the magnetic spectrometer. The PMQ triplet is nominally aligned to the axis of the drive laser and therefore the electron beam. However, if the electron beam does not travel along the exact magnetic axis of the PMQ triplet, it will acquire a net transverse kick in the direction of misalignment. Naturally, the transverse kick will be energy dependent and manifest in the form of dispersion as the beam propagates. A beam with an initial vertical position and/or angular offset to the magnetic axis of the PMQ triplet will accrue some energy dependent dispersion η_y and appear tilted vertically at the magnetic spectrometer which disperses the beam horizontally. Although positional and angular offsets of the beam relative to the PMQ axis will induce dispersion, it is not likely to be the only source. For example, asymmetries in the laser profile or inhomogeneities in the plasma can induce asymmetric wakefields which themselves impart transverse kicks to the accelerating beam. It is therefore possible for LPA beams to be born with some nonzero dispersion at the source. Taking all of the above into account, we can write a function describing the vertical dispersion at the reference energy of 108 MeV at the location of the magnetic spectrometer $\eta_{y,f}$ as

$$\eta_{y,f}\left[\frac{\mu\text{m}}{\Delta\text{MeV}}\right] = \alpha y_i' + \beta y_i + g(\mathcal{O}), \quad \text{with} \quad y_i' = y_{\text{laser}}' + h(\mathcal{O}). \tag{3}$$

The coefficients α and β are directly calculated from the transfer matrix R and found to be $\alpha = -65$ mrad^{-1} and $\beta = 0.26$ μm^{-1}. For the laser system used in this work, with ≈ 100 s of μrad jitter in angle y_{laser}' and ≈ 10 μm jitter in position y_{laser}, the angular jitter has a larger impact on the final dispersion than the positional jitter. Here $g(\mathcal{O})$ represents any dispersion originating from the source itself, whereas $h(\mathcal{O})$ represents contributions to the exit of the angle not directly tied to the angle of the drive laser.

Equations (2) and (3) indicate the experimental observables of vertical position $y_f(\gamma_0)$ and vertical dispersion $\eta_{y,f}$ at the spectrometer is directly linked to the laser position y_{laser} and angle y_{laser}' at focus. Minimizing the fluctuations of these parameters will therefore directly improve the electron beam transverse source stability. Example images of the LPA generated electron beams transported to the magnetic spectrometer are shown in Fig. 2, where the electrons are dispersed in energy along the horizontal axis.

The characteristic "bow-tie" shape is a direct result of the energy dependent transport summarized in Eq. (1). In the top figure, the e-beam is well centered on the nominal axis and exhibits very little dispersion in the vertical plane; a good indication the e-beam is well aligned. In the bottom figure, the beam at 108 MeV is offset from the vertical axis by 850 μm and has a vertical tilt that indicates 22 μm/MeV dispersion. Note that for 108 MeV $R_{33} = -39.6$, which indicates a magnification factor of ×39.6. Thus, the measured 850 μm offset indicates a 20-μm vertical shift in the laser focal position, which matches the measured shift of the high power "ghost beam" shown in the figure.

IV. RESULTS OF ACTIVE STABILIZATION

In Fig. 3, we show a sequence of measurements of e-beam vertical position and dispersion at the imaged energy of 108 MeV, in which we alternate enabling and disabling the active stabilization system over the course of 1 h. During this period, the integrated rms error with the feedback on vs off was 125 and 481 μm for position, respectively, and 32 and 40 μm/MeV for dispersion, respectively. Taking the R_{33} magnification factor into account, position fluctuations were reduced and locked to 3 μm over the course of the hour. Uncertainty in the determination of the position and angle of the ghost beam can arise due to shot-to-shot modal and intensity fluctuations in the beam profile which can affect the calculation of the centroid. We have estimated these quantities to be < 3 μm for position and ∼70 μrad for angle. We also cross referenced our angle measurement technique with a wavefront sensor that reports a 10-μrad error and found a similar level of error in the ghost angle measurement, e.g., ∼70 μrad.

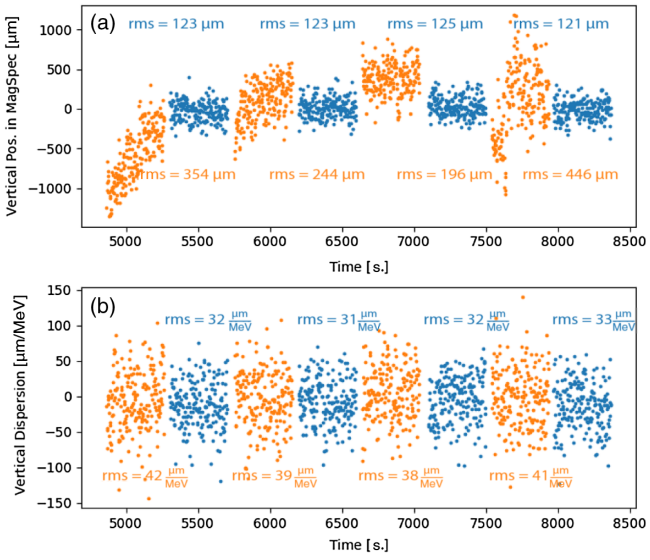

FIG. 3. Four sets of the feedback stabilization system on (blue) vs off (orange) and their corresponding e-beam source vertical position (a) and dispersion (b) in the magnetic spectrometer were measured. The integrated rms error with the feedback on vs off was 125 and 481 μm for position, and 32 and 40 μm/MeV for dispersion with the feedback on and off, respectively. We note that the active stabilization is reducing both shot-to-shot variation and long-term drift.

The improvement in dispersion compared to the position is less and is related to the fact that the e-beam angle can be influenced by other factors such as wakefield asymmetry and/or off-axis particle injection. In these cases, the beam can undergo transverse oscillations around the nominal accelerator axis due to the transverse focusing associated with the wakefield. The final betatron phase at the plasma exit will be a function of the detailed plasma profile, and small shot-to-shot variations in the profile can result in variations in the exit angle of the electron beam relative to the drive laser axis. The improvement in dispersion jitter does, however, paint a clear picture that the angular jitter of the e-beam has been reduced. If we make the reasonable assumption that the jitter in the last term on the rhs of Eq. (3) is independent of variations in drive laser position and angle, then the reduction in angular jitter of the e-beam via stabilization of the wakefield driving laser is given as

$$\sqrt{\Delta\sigma_{y_i'}^2} = 1/\alpha\sqrt{\Delta\sigma_{\eta_{y,f}}^2 - \beta^2\Delta\sigma_{y_i}^2}, \tag{4}$$

where the capital Deltas represent the difference in the variance between the stabilization off/on measurements of the corresponding value. Substituting the appropriate physical measurements into Eq. (4) shows a reduction of a statistically independent source of e-beam angular jitter due to drive laser instabilities of ∼0.37 mrad—a value that closely agrees with our reduction in laser angle jitter. Moreover, this result validates the claim made in Eq. (3) that the pointing fluctuations of the wakefield driving laser couple, largely independently, with the effects described by the big-O-notation terms into e-beam angle and dispersion jitter. This substantiates the need to better understand and control these other sources of jitter in order to further improve salient properties of LPA-generated e-beams. In regard to energy stability, we observed no improvement in the spectrum of the e-beam. This is largely due to the plasma density not significantly varying over the relative spatial scales in which we are seeing improvement to drive laser stability—and also due to the intrinsic large energy spread/stability associated with ionization ejection in LPAs [28].

Meanwhile, following Eqs. (2) and (3), Fig. 4 demonstrates the reduced dependence between e-beam and drive laser stability when feedback stabilization is on through correlation analysis. A stronger reduction in correlation when active stabilization is on vs off implies better performance from the active stabilization system. We note the apparent difference in performance in terms of a residual correlation term between active stabilization of

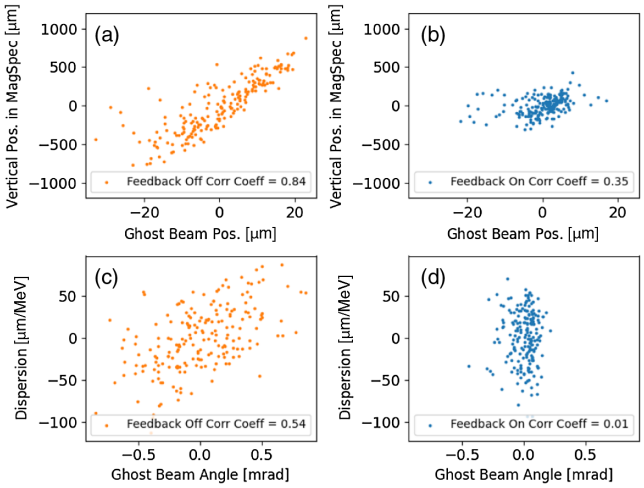

FIG. 4. Correlation between the ghost beam and the e-beam for both angle (a,b) and position (c,d) is shown when the feedback is on and off. We note the active stabilization system's ability to practically eliminate any dependence between e-beam dispersion and drive-laser angle while also displaying an encouraging reduction in positional dependence. Greater reduction in correlation implies better performance from the stabilization system.

the position vs the angle. This is due to the presence of higher frequency oscillations in the position spectrum that are absent in the angle spectrum of the drive-laser [1]—a confirmation of the low-bandwidth limitation associated with the active stabilization system. It does, however, paint the encouraging notion that further improvement to closed-loop stabilization technologies will result in further improvement to laser, and thus LPA, stability.

Overall, the online, nondestructive stabilization system using signals from a ghost copy of the unamplified kHz pulse train has yielded direct and substantial improvement in the transverse stability of electron beams. It is well known that keeping the e-beam close to the design axis is of critical importance for the future success of high impact but demanding applications like light sources or particle colliders. These results are encouraging for the future of plasma based particle accelerators by improving the intrinsic shot-to-shot stability.

V. CONCLUSION

An active stabilization system was installed on a 100-TW-class pulsed-laser system used for the production of LPA-generated e-beams. The system was based on an optical design that allows for the extraction of a nondestructive ghost beam copy of the main kHz pulse train. The ghost beam was then sent to a monitoring setup used to diagnose and correct for oscillatory behavior of the LPA drive laser through the use of an active feedback stabilization system. By examining the imaged e-beam in a magnetic spectrometer, we have demonstrated that stabilization of the LPA drive-laser resulted in improved shot-to-shot e-beam transverse stability and dispersion.

ACKNOWLEDGMENTS

This work was supported by the U.S. Department of Energy (DOE), Office of Science, the Office of High Energy Physics, under Contract No. DE-AC02-05CH11231. K. Jensen participated in the research at LBNL as a University of Nebraska student through the DOE Office of Science Graduate Student Research (SCGSR) program, administered by the Oak Ridge Institute for Science and Education under Contract No. DE-SC0014664.

[1] F. Isono, J. van Tilborg, S. K. Barber, J. Natal, C. Berger, H.-E. Tsai, T. Ostermayr, A. Gonsalves, C. Geddes, and E. Esarey, High Power Laser Sci. Eng. **9** (2021).
[2] E. Esarey, C. B. Schroeder, and W. P. Leemans, Rev. Mod. Phys. **81**, 1229 (2009).
[3] T. Tajima and J. M. Dawson, Phys. Rev. Lett. **43**, 267 (1979).
[4] X. Wang, R. Zgadzaj, N. Fazel, Z. Li, S. Yi, X. Zhang, W. Henderson, Y.-Y. Chang, R. Korzekwa, H.-E. Tsai *et al.*, Nat. Commun. **4**, 1988 (2013).
[5] W. Leemans, A. Gonsalves, H.-S. Mao, K. Nakamura, C. Benedetti, C. Schroeder, C. Tóth, J. Daniels, D. Mittelberger, S. Bulanov *et al.*, Phys. Rev. Lett. **113**, 245002 (2014).
[6] W. P. Leemans, B. Nagler, A. J. Gonsalves, C. Tóth, K. Nakamura, C. G. Geddes, E. Esarey, C. Schroeder, and S. Hooker, Nat. Phys. **2**, 696 (2006).
[7] A. J. Gonsalves *et al.*, Phys. Rev. Lett. **122**, 084801 (2019).
[8] A. Rousse, K. T. Phuoc, R. Shah, A. Pukhov, E. Lefebvre, V. Malka, S. Kiselev, F. Burgy, J.-P. Rousseau, D. Umstadter, and D. Hulin, Phys. Rev. Lett. **93**, 135005 (2004).
[9] A. E. Hussein *et al.*, Sci. Rep. **9**, 3249 (2019).
[10] W. Wang, K. Feng, L. Ke, C. Yu, Y. Xu, R. Qi, Y. Chen, Z. Qin, Z. Zhang, M. Fang, J. Liu, K. Jiang, H. Wang, C. Wang, X. Yang, F. Wu, Y. Leng, J. Liu, R. Li, and Z. Xu, Nature (London) **595**, 516 (2021).
[11] K. Ta Phuoc, S. Corde, C. Thaury, V. Malka, A. Tafzi, J. P. Goddet, R. C. Shah, S. Sebban, and A. Rousse, Nat. Photonics **6**, 308 (2012).
[12] H. Schwoerer, B. Liesfeld, H.-P. Schlenvoigt, K.-U. Amthor, and R. Sauerbrey, Phys. Rev. Lett. **96**, 014802 (2006).
[13] R. W. Assmann, Eur. Phys. J. Spec. Top. **229**, 3675 (2020).
[14] G. White and T. Raubenheimer, Transverse jitter tolerance issues for beam-driven plasma accelerators, SLAC National Accelerator Laboratory, Menlo Park, CA, Technical Report, 2019.
[15] L. T. Ke, K. Feng, W. T. Wang, Z. Y. Qin, C. H. Yu, Y. Wu, Y. Chen, R. Qi, Z. J. Zhang, Y. Xu, X. J. Yang, Y. X. Leng, J. S. Liu, R. X. Li, and Z. Z. Xu, Phys. Rev. Lett. **126**, 214801 (2021).
[16] G. Genoud, F. Wojda, M. Burza, A. Persson, and C.-G. Wahlström, Rev. Sci. Instrum. **82**, 033102 (2011).
[17] A. Popp, J. Vieira, J. Osterhoff, Z. Major, R. Hörlein, M. Fuchs, R. Weingartner, T. P. Rowlands-Rees, M. Marti,

R. A. Fonseca, S. F. Martins, L. O. Silva, S. M. Hooker, F. Krausz, F. Grüner, and S. Karsch, Phys. Rev. Lett. **105**, 215001 (2010).

[18] Y. Ma, D. Seipt, S. J. D. Dann, M. J. V. Streeter, C. A. J. Palmer, L. Willingale, and A. G. R. Thomas, Phys. Plasmas **25**, 113105 (2018).

[19] J. Faure, C. Rechatin, A. Norlin, A. Lifschitz, Y. Glinec, and V. Malka, Nature (London) **444**, 737 (2006).

[20] A. R. Maier, N. M. Delbos, T. Eichner, L. Hübner, S. Jalas, L. Jeppe, S. W. Jolly, M. Kirchen, V. Leroux, P. Messner, M. Schnepp, M. Trunk, P. A. Walker, C. Werle, and P. Winkler, Phys. Rev. X **10**, 031039 (2020).

[21] S. Corde, C. Thaury, A. Lifschitz, G. Lambert, K. Ta Phuoc, X. Davoine, R. Lehe, D. Douillet, A. Rousse, and V. Malka, Nat. Commun. **4**, 1501 (2013).

[22] C. Rechatin, J. Faure, A. Ben-Ismail, J. Lim, R. Fitour, A. Specka, H. Videau, A. Tafzi, F. Burgy, and V. Malka, Phys. Rev. Lett. **102**, 164801 (2009).

[23] C. B. Schroeder, E. Esarey, C. G. R. Geddes, C. Benedetti, and W. P. Leemans, Phys. Rev. ST Accel. Beams **13**, 101301 (2010).

[24] M. Couprie, J. Electron Spectrosc. Relat. Phenom. **196**, 3 (2014).

[25] S. Corde, K. Ta Phuoc, G. Lambert, R. Fitour, V. Malka, A. Rousse, A. Beck, and E. Lefebvre, Rev. Mod. Phys. **85**, 1 (2013).

[26] C. McGuffey, A. G. R. Thomas, W. Schumaker, T. Matsuoka, V. Chvykov, F. J. Dollar, G. Kalintchenko, V. Yanovsky, A. Maksimchuk, K. Krushelnick, V. Y. Bychenkov, I. V. Glazyrin, and A. V. Karpeev, Phys. Rev. Lett. **104**, 025004 (2010).

[27] A. Pak, K. A. Marsh, S. F. Martins, W. Lu, W. B. Mori, and C. Joshi, Phys. Rev. Lett. **104**, 025003 (2010).

[28] S. Bohlen, J. C. Wood, T. Brümmer, F. Grüner, C. A. Lindstrøm, M. Meisel, T. Staufer, R. D'Arcy, K. Põder, and J. Osterhoff, Phys. Rev. Accel. Beams **25**, 031301 (2022).